Proceedings of IMECE2006
2006 ASME International Mechanical Engineering Congress and Exposition
November 5-10, 2006, Chicago, Illinois, USA

IMECE2006-14542

SMART MATERIAL ELECTROHYDROSTATIC ACTUATOR FOR INTELLIGENT TRANSPORTATION SYSTEMS

Michael J. Rupinsky
Smart Materials and Structures Laboratory
Department of Mechanical Engineering
The Ohio State University
Columbus, Ohio 43202

Marcelo J. Dapino*
Smart Materials and Structures Laboratory
Department of Mechanical Engineering
The Ohio State University
Columbus, Ohio 43202
dapino.1@osu.edu

ABSTRACT

Future intelligent transportation systems require actuation systems that are lightweight, compact and have a large power density. Due to their solid-state operation, fast frequency response, and high power-to-weight ratio, electrohydrostatic actuators based on smart materials are attractive as a replacement for conventional hydraulic actuators. This paper is focused on the development of a smart material pump for EHAs in which mechanical vibrations produced by a magnetostrictive terbium-iron-dysprosium alloy are rectified by means of diode-type mechanical reed valves. A maximum blocked pressure differential of 1100 psi is achieved with a power consumption of 84 W. A linear dynamic system model of the magnetostrictive pump is presented. The linear model quantifies the maximum pressure and electromechanical coupling of the magnetostrictive pump and facilitates the determination of system parameters from simple experimental measurements.

INTRODUCTION

The increased use of electrically operated actuators as a replacement for hydraulic devices in automotive suspension, steering, and braking systems motivates the development of advanced "fly-by-wire" actuators capable of large forces, large displacements, and fast responses. While smart materials can produce large forces over broad frequency bandwidths, they only produce very small displacements. An electrohydrostatic actuator (EHA) operates on the principle of fluid flow rectification and consists of a piezoelectric or magnetostrictive pump, rectification valves, and hydraulic piston (Fig. 1).

Bridger et al. [1] developed a magnetostrictive pump capable of producing 3000 psi with an electromechanical coupling of 60%. The pump relies on inertial resonant motion of the pump body to produce high pressure. Several piezoelectric pumps have been constructed that rely on standard mechanical/passive check valves with a bandwidth of approximately 200-400 Hz. Sirohi and Chopra [2] compared the operation of a piezo-hydraulic pump with standard ball and cone check valves to reed valves and concluded that the reed valves allow for higher pumping frequencies up to 1 kHz. Chapman et al. [3] developed three small piezo-hydraulic pumps with the smallest weighing only 90 grams and capable of 600 psi of blocked pressure and 45 cc/min at 60 Hz. Another design produces a blocked pressure of 250 psi (over the bias pressure) and a flow of 338 cc/min when driven at 400 Hz.

Oates and Lynch [4] presented a state space model for a piezoelectric hydraulic pump and used the model as a design tool for subsequent pump designs. The differential equations of each subsystem were coupled and solved simultaneously to obtain the overall system response. Sirohi et al. [5] used transfer matrix analysis to model the dynamics of a piezo-hydraulic actuator, specifically the effects of viscosity and fluid transmission lines. Their analysis shows that increasing the tube length reduces the resonant frequency of the system and fluid viscosity affects the system in a manner similar to viscous damping. Downey and Dapino [6] presened a hybrid Terfenol-D/PMN-PT transducer and model that provides accurate simulations of electromechanical transducer behavior and also a framework for material property characterization.

*Address all correspondence to this author.

This paper presents (i) a magnetostrictive pump for an electrohydrostatic actuator in which magnetostrictive vibrations are amplified to produce large deformations and forces and (ii) a dynamic system model that characterizes the fluid network coupled to the electromechanical transducer. Amplification of the magnetostrictive vibrations is achieved by utilizing hydraulic advantage to convert magnetostrain into large forces and mechanical reed valves to rectify the oscillatory pressure flow from the magnetostrictive vibrations, resulting in high-pressure unidirectional flow. The dynamic system model is meant as a tool for the design, analysis and control of the device. Calculation of mechanical and electrical impedances allows to analyze the effect of hydraulic loading on pump operation.

Magnetostrictive materials are nonlinear and hysteretic but can be assumed to be linear at low-signal regimes. From this assumption, a linear model is developed that couples the electrical, mechanical and fluid domains and can be used to model the overall system response. A lumped parameter analysis and Newton's laws couple the mechanical and fluid domains, electroacoustic transduction equations provide coupling between mechanical and electrical domains and piezomagnetic constitutive equations relate the material properties with electromechanical transduction coefficients.

THEORY

The fluid network associated with the magnetostrictive pump being investigated in this paper is represented by the schematic in Fig. 1. A dynamic system model which describes the relationships between the electrical, mechanical and fluid subsystems of the Terfenol-D pump is presented. The model characterizes the pump in two ways: (i) system operation, i.e., system pressure and actuator velocity and displacement, is described for a given harmonic input and (ii) dynamic characteristics of the Terfenol-D pump, i.e., various parameters affecting the electrical drive-point impedance, are developed through an electrical impedance analysis. First, the coupled equations of motion for the mechanical and fluid subsystems are derived separately. The differential equations for each subsystem are then assembled into a system matrix and state space techniques are utilized to solve the system matrix for a given harmonic input. Last, an expression is developed for the electrical drive-point impedance relating the electrical and mechanical domains through manipulation of electroacoustic transduction equations for electromechanical transducers and piezomagnetic constitutive equations. The electroacoustic portion of the dynamic system model uses a superposition of results obtained from the harmonic portion of the model along with an evaluation of the electrical impedance in order to obtain the desired characteristics.

Mechanical Modeling

In order to take full advantage of the magnetomechanical coupling, Terfenol-D must be utilized in a transducer comprising a magnetic circuit and mechanical preload. The Terfenol-D transducer is similar to typical Terfenol-D transducer designs in that the pushrod acts as a piston by pushing against a thin stainless steel diaphragm and producing volume flow. Terfenol-D provides the mechanical stiffness and damping of this system and generates the mechanical driving force through magnetostrictive vibrations. The stiffness of a Terfenol-D rod is related to the Young's modulus E_y^H and the geometry of the rod by $k_t = E_y^H A_t / L_t$, where A_t is the cross-sectional area and L_t is the length of the rod. The damping coefficient is more difficult to define. Since the Terfenol-D transducer is coupled to a hydraulic circuit, there are fluid stiffness, damping and inertia effects of the pumping chamber that must be taken into account.

The Terfenol-D pump and fluid column inside the pump chamber are modeled as a second order, two degree of freedom spring-mass-damper system (Fig. 2). The fluid column is in contact with both the piston and the pumping chamber ceiling and thus fixed with respect to these two planes. The vibratory model accounts for the mechanical stiffness and damping coefficients of Terfenol-D as well as the fluid damping, stiffness and inertance of the hydraulic oil in the pumping chamber. The two degrees of freedom arise from motion of the effective mass of the Terfenol-D rod m_i and the mass of the column of fluid m_f. The effective mass includes the dynamic mass of the Terfenol-D rod and mass of the piston and diaphragm. The mechanical stiffness and damping of the Terfenol-D transducer behave as the parallel combination of a spring k_i and damper b_i. It is noted that $k_i = k_t + k_d$ and $b_i = b_t + b_d$, where the subscripts refer to Terfenol-D and the stainless steel diaphragm respectively. The fluid stiffness k_f and damping b_f are modeled as described in Fig. 2 in order to account for the fluid contact with the piston and chamber wall. The two forces on the subsystem are the force generated by the magnetostrain of the Terfenol-D element, αI, which is related to the input current through the electroacoustic relations and the force applied to the mass of the fluid due to the pressure inside the pumping chamber, $F_{ext} = P_1 A_i$ where A_i is the cross-sectional area of the pumping chamber. The magnetostrictive subsystem is coupled to the fluid domain through the pressure P_1. The equation of motion of each mass is solved by using Newton's second law and written in terms of the velocity and displacement state variables (x_t, v_t, x_f, v_f),

$$m_i \dot{v_t} + \left(b_i + \frac{b_f}{2}\right) v_t - \frac{b_f}{2} v_f + \left(k_i + \frac{k_f}{2}\right) x_t - \frac{k_f}{2} x_f = \alpha I \quad (1)$$

$$m_f \dot{v_f} - \frac{b_f}{2} v_t + b_f v_f - \frac{k_f}{2} x_t + k_f x_f = -P_1 A_i \quad (2)$$

where the fluid stiffness is defined by the bulk modulus of the hydraulic fluid, β, the cross-sectional area of the pumping chamber and the height h of the pumping chamber, $k_f = \beta A_i / h$.

To fully characterize the system, it is necessary to quantify the effects of loading on the behavior of the transducer. Changes in the fluid loading will affect the dynamic characteristics of the Terfenol-D transducer. As a means to fully describe the mechanical regime of the transducer, the frequency response function

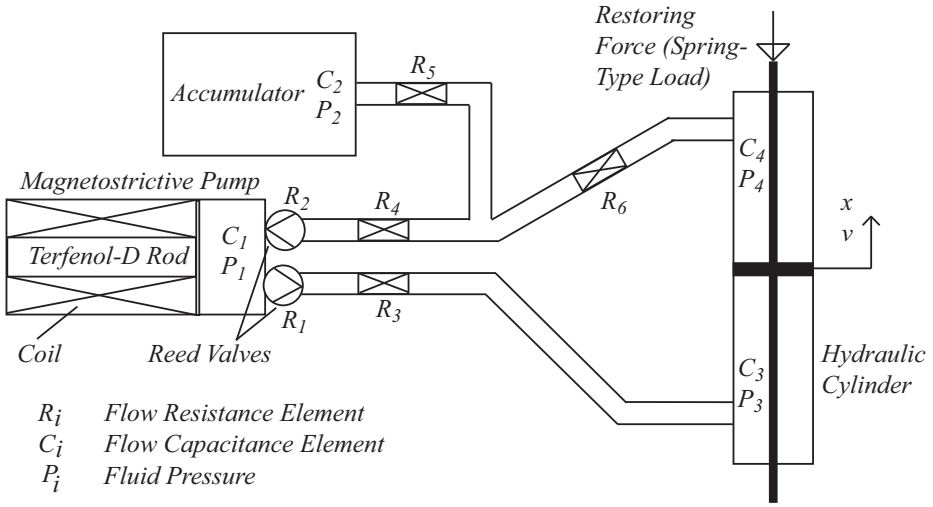

Figure 1. UNIDIRECTIONAL ELECTROHYDRAULIC ACTUATOR. AN EXTERNAL SPRING-TYPE LOAD PROVIDES THE RESTORING FORCE.

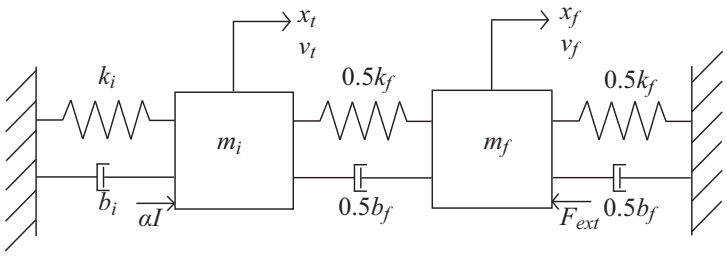

Figure 2. TWO DEGREE OF FREEDOM VIBRATORY MODEL OF THE MAGNETOSTRICTIVE PUMP.

force per velocity, i.e. the mechanical impedance Z_{mech}, can be found for the Terfenol-D portion of the transducer. To quantify the mechanical impedance, the external loading due to the fluid is assumed zero and the force per Terfenol-D velocity is calculated,

$$Z_{mech} = \frac{\alpha I}{v_t} = \frac{m_i(j\omega)^2 + b_i j\omega + k_i}{j\omega}. \tag{3}$$

The fluid portion removed in this calculation is defined as the load impedance connected to the transducer.

Fluid Modeling

The fluid network shown in Fig. 1 is used to derive the equations of motion that govern the fluid flow through the pump and fluid network. The oscillatory fluid flow inside the pumping chamber produced by the magnetostrictive pump is rectified by custom-made reed valves. The reed valves are stainless steel flaps that can only deform in the direction of fluid flow. Figure 3 illustrates the reed valve operation. A positive pressure gradient across the reed valve deforms the reed and allows flow. A negative pressure gradient pushes the reed against the fluid orifice and effectively blocks the flow. This behavior can be represented as a finite fluid resistance in the direction of allowed flow and infinite fluid resistance otherwise. An accumulator is placed on the low pressure side of the pump and provides a bias pressure on the fluid. The bias pressure prevents fluid cavitation and supplies the pumping chamber with fluid after each stroke of the Terfenol-D transducer. The hydraulic cylinder transmits the force produced by the magnetostrictive pump to an external mechanical load. A lumped parameter analysis is used to derive the fluid differential equations of the four pressure states in the hydraulic circuit (P_1,

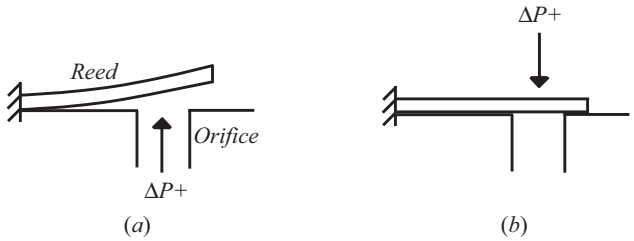

Figure 3. CROSS-SECTIONAL VIEW OF A REED VALVE. (a) FOR A POSITIVE PRESSURE GRADIENT IN THE DESIRED DIRECTION OF FLUID FLOW, THE REED FLAP DEFLECTS AND ALLOWS FLUID FLOW. (b) FOR A POSITIVE PRESSURE GRADIENT IN THE OPPOSITE DIRECTION, THE REED FLAP BLOCKS THE ORIFICE AND ALLOWS NO FLOW.

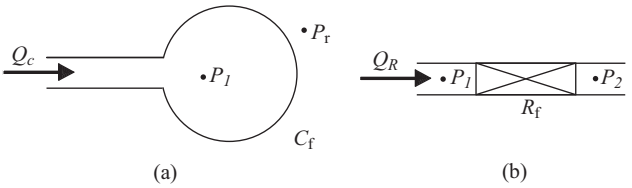

Figure 4. SYMBOLIC DIAGRAMS OF (a) A FLUID CAPACITOR AND (b) A FLUID RESISTOR. [7]

P_2, P_3, P_4). The elemental equations for ideal fluid capacitors and flow resistors are described in terms of pressure and volume flow rate as in Fig. 4,

$$Q_c = C_f \frac{dP_{1r}}{dt} \tag{4}$$

$$P_{12} = R_f Q_R \tag{5}$$

with pressure drops P_{1r} and P_{12}, volume flow rates Q_c and Q_R, fluid capacitance C_f, flow resistance R_f defined as [7]

$$C_f = \frac{V_c}{\beta} \tag{6}$$

$$R_f = \frac{128\mu_f L}{\pi d^4}. \tag{7}$$

Here V_c is the volume of the fluid cavity, β is the bulk modulus of the hydraulic fluid, μ_f is the dynamic fluid viscosity, and L and d are the length and diameter of the fluid line. The fluid interconnection laws of continuity and compatibility, analogous to Kirchoff's laws for electrical circuits, are used to derive the differential equations for the pressure state variables. The law of continuity states that the sum of the volume flow rates at any node must be zero and the law of compatibility states that the sum of the pressure drops around a closed loop is zero. There are four fluid capacitors each corresponding to one of the four pressure states and a fluid resistor for each line resistance. The inertance of the column of fluid in the pumping chamber is modeled in the mechanical domain; considering the relatively low mass density and volume of the hydraulic fluid in the fluid lines, the inertance and capacitance of the fluid lines are assumed negligible.

The velocity of the fluid mass provides the input hydraulic flow for the hydraulic circuit. The output cylinder motion is dependent on the pressure states on either side of the piston and is modeled as a single degree of freedom system in terms of the output position and velocity (x_o, v_o) of the piston.

State Space Modeling

State space analysis is used to solve the portion of the dynamic system model coupling the mechanical and fluid domains of the pump. Newton's second law and the fluid interconnection laws are used to derive the coupled mechanical and fluid equations for the pump. The mechanical equations of motion include both displacement and velocity state variables. By adding the velocity state variables in the mechanical equations of motion, each second order equation is broken into two first order equations resulting in a complete system of first order equations. This allows simplification of the model in that only one system matrix is needed for obtaining a solution. Since the mechanical and fluid equations of motion are coupled, simultaneous solutions are required. The complete system level model, represented as a matrix state equation with system matrix $[A]$, input matrix $[B]$, state vector $\vec{x}(t)$ and forcing vector $\vec{u}(t)$, is solved using the convolution (superposition) integral,

$$\dot{\vec{x}}(t) = [A]\vec{x}(t) + [B]\vec{u}(t) \tag{8}$$

$$\vec{x}(t) = e^{[A](t-t_0)}\vec{x}(t_0) + \int_{t_0}^{t} e^{[A](t-\tau)}[B]\vec{u}(\tau)d\tau. \tag{9}$$

The solution is assumed to consist of two parts: (i) a free component $\vec{x}_{free}$ which is the solution of the matrix state equation for the forcing vector at time $t = t_0$ and initial conditions $\vec{x}(t_0)$, and (ii) a forced component $\vec{x}_{forced}$ for the forcing input $\vec{u}(t)$ with zero initial state [8]. The matrix state equation is solved for each time step using the previous solution as its initial condition. Since the solution is found using a linear superposition solver, the time step must be small enough so that the changes between steps can be assumed linear. Time steps that are too large may result in inaccurate and often unstable solutions.

The differential equations of the fluid and mechanical subsystems are derived separately and then combined to form the system matrix $[A]$. The matrix state equation for the Terfenol-D pump is given by Eqn. (10) and is assembled in MATLAB. The dynamic system model is solved using the superposition solver 'lsim', which gives the time response of the matrix state equation. An algorithm is written describing the fluid diode behavior of the reed valves by using the pressure states across the reed valves to determine the value of the reed valve resistance. Since the capacitance of the fluid capacitors C_3 and C_4 in the hydraulic cylinder have varying heights with respect to output actuator motion, they depend on the value of the hydraulic cylinder displacement. The values of the reed valve resistances and fluid capacitors C_3 and C_4 are determined before each solution, depending on the pressure and actuator displacement states.

Electroacoustics Theory

In describing the coupling between the electrical and mechanical domains of the Terfenol-D pump, classical electroacoustic transduction theory is considered, assuming linear transducer operation [9]. Figure 5 illustrates a transduction model for general electromechanical devices. This model is used to derive two equations that couple the electrical and mechanical domains,

$$V = Z_e I + T_{em} v_t \tag{13}$$

$$F = T_{me} I + Z_m v_t, \tag{14}$$

$$\begin{bmatrix} \dot{x}_t \\ \dot{v}_t \\ \dot{x}_f \\ \dot{v}_f \\ \dot{P}_1 \\ \dot{P}_2 \\ \dot{P}_3 \\ \dot{P}_4 \\ \dot{x}_o \\ \dot{v}_o \end{bmatrix} = \begin{bmatrix} 0 & 1 & 0 & 0 & 0 & 0 & 0 & 0 & 0 & 0 \\ \frac{-(2k_i+k_f)}{2m_i} & \frac{-(2b_i+b_f)}{2m_i} & \frac{k_f}{2m_i} & \frac{b_f}{2m_i} & 0 & 0 & 0 & 0 & 0 & 0 \\ 0 & 0 & 0 & 1 & 0 & 0 & 0 & 0 & 0 & 0 \\ \frac{k_f}{2m_f} & \frac{b_f}{2m_f} & \frac{-k_f}{m_f} & \frac{-b_f}{m_f} & \frac{-A_i}{m_f} & 0 & 0 & 0 & 0 & 0 \\ 0 & 0 & 0 & \frac{A_i}{C_1} & K & \frac{R_6}{C_1 R_{eqv}} & \frac{1}{C_1(R_1+R_3)} & \frac{R_5}{C_1 R_{eqv}} & 0 & 0 \\ 0 & 0 & 0 & 0 & \frac{R_6}{C_2 R_{eqv}} & \frac{R_6(R_2+R_4)-R_{eqv}}{C_2 R_5 R_{eqv}} & 0 & \frac{R_2+R_4}{C_2 R_{eqv}} & 0 & 0 \\ 0 & 0 & 0 & 0 & \frac{1}{C_3(R_1+R_3)} & 0 & \frac{-1}{C_3(R_1+R_3)} & 0 & 0 & \frac{-A_o}{C_3} \\ 0 & 0 & 0 & 0 & \frac{R_5}{C_4 R_{eqv}} & \frac{R_2+R_4}{C_4 R_{eqv}} & 0 & \frac{R_5(R_2+R_4)-R_{eqv}}{C_4 R_6 R_{eqv}} & 0 & \frac{A_o}{C_4} \\ 0 & 0 & 0 & 0 & 0 & 0 & 0 & 0 & 0 & 1 \\ 0 & 0 & 0 & 0 & 0 & 0 & \frac{A_o}{m_o} & \frac{-A_o}{m_o} & 0 & \frac{-b_o}{m_o} \end{bmatrix} \begin{bmatrix} x_t \\ v_t \\ x_f \\ v_f \\ P_1 \\ P_2 \\ P_3 \\ P_4 \\ x_o \\ v_o \end{bmatrix} + \begin{bmatrix} 0 \\ \frac{-T_{me}}{m_i} \\ 0 \\ 0 \\ 0 \\ 0 \\ 0 \\ 0 \\ 0 \\ 0 \end{bmatrix} I \quad (10)$$

$$R_{eqv} = (R_2+R_4)(R_5+R_6)+R_5R_6 \quad (11)$$

$$K = \frac{R_5R_6(R_1+R_3)-R_{eqv}(R_1+R_2+R_3+R_4)}{C_1R_{eqv}(R_1+R_3)(R_2+R_4)} \quad (12)$$

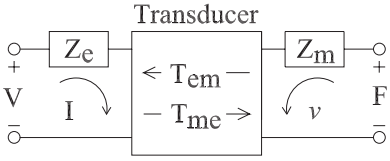

Figure 5. SCHEMATIC REPRESENTATION OF AN ELECTROMECHANICAL SYSTEM. [9]

where V is the applied voltage to the transducer, I is the current flow through the transducer, F is the force on the transducer, v_t is the velocity, Z_e and Z_m are the blocked electrical and mechanical impedances, and T_{em} and T_{me} are transduction coefficients that describe the electromechanical coupling. The subscripts em and me refer to 'electrical due to mechanical' and 'mechanical due to electrical' energy transduction processes. The blocked electrical impedance is the measured impedance that occurs when the output motion of the Terfenol-D is completely blocked.

Important transducer characteristics are revealed by studying the electrical drive-point impedance which is defined as the complex ratio of voltage to current. In typical transducer applications described by Eqn. (13)–(14), the force F is connected to a mechanical load impedance Z_L defined as

$$F \equiv -Z_L v_t. \quad (15)$$

The definition of load impedance is substituted into Eqn. (14) and the velocity is written as

$$v_t = -\frac{T_{me}I}{Z_m+Z_L}. \quad (16)$$

Eqn. (16) is then substituted into equation (13) in order to find an expression for the electrical drive-point impedance Z_{ee},

$$Z_{ee} = \frac{V}{I} = Z_e + \frac{-T_{em}T_{me}}{Z_m+Z_L} = Z_e + Z_{mot}. \quad (17)$$

The electrical drive-point impedance is the sum of the blocked electrical impedance Z_e and motional impedance Z_{mot} which quantifies the electromechanical coupling of the transducer.

Electroacoustic Equations. The linear piezomagnetic constitutive relations combine the elastic and magnetic effects on the strain ε and magnetic induction B of Terfenol-D,

$$\varepsilon = s^H\sigma + qH \quad (18)$$

$$B = q^*\sigma + \mu^\sigma H, \quad (19)$$

where σ is the stress on the Terfenol-D rod, H is the magnetic field through the rod, s^H is the elastic compliance at constant magnetic field, $q = q^*$ are piezomagnetic coupling coefficients, and μ^σ is the magnetic permeability at constant stress. In Eqn. (18) the strain is represented by the superposition of Hooke's law $\varepsilon = s^H\sigma$ and the magnetostrictive contribution qH. In Eqn. (19) the magnetic induction is the superposition of a magnetic term $B = \mu H$ and a mechanically coupled term $q^*\sigma$. The constitutive relations are manipulated into the form of the electroacoustic equations by utilizing additional electro-magneto-mechanical relations. It is assumed that the Terfenol-D rod completely fills an ideal wire solenoid of N turns, length L_t and cross-

sectional area A_t and that the current and magnetic field are linearly related [6]. The total flux through the rod is $\phi = BA_t$ and the flux linkage is $\lambda = NBA_t$. Assuming spatial independence of stress and strain, the strain in the Terfenol-D rod is related to the displacement x_t by definition $\varepsilon \equiv x_t/L_t$, and can be expressed in terms of velocity through its derivative. The stress on the rod is related to the force through the ratio of the cross-sectional area of the rod. The total voltage drop across the coil is the series combination of an electrical DC resistance and inductance. These relationships are mathematically expressed in the following form

$$H = nI \tag{20}$$

$$\varepsilon = \frac{v_t}{j\omega L_t} \tag{21}$$

$$\sigma = \frac{F}{A_t} \tag{22}$$

$$V = R + j\omega NBA_t, \tag{23}$$

where $n = N/L_t$ is the turns ratio of the drive coil. The electroacoustic equations relating the input voltage and output force with respect to input current and output velocity for a Terfenol-D driven pump are thus formed [6],

$$V = [R + j\omega\mu^{\sigma}(1-k^2)n^2A_tL_t]I + Nqk_tv_t \tag{24}$$

$$F = -Nqk_tI + \frac{k_t}{j\omega}v_t. \tag{25}$$

By comparison with the electroacoustic equations (13)-(14) it is apparent that the blocked electrical impedance is the electrical series combination of an ideal resistor and inductor with inductance L_{block} expressed in terms of material properties,

$$Z_e = R + j\omega\mu^{\sigma}(1-k^2)n^2A_tL_t = R + j\omega L_{block}. \tag{26}$$

The electromechanical transduction coefficients and blocked mechanical impedance are equivalently identified as $T_{me} = -T_{em} = -Nqk_t$ and $Z_m = k_t/j\omega$. The transduction coefficients are equal in magnitude and opposite in direction in agreement with theory of magnetostrictive transduction [9].

Modified Blocked Impedances. The expressions developed for the blocked mechanical and electrical impedances present a model that does not adequately describe the behavior of the Terfenol-D pump. Firstly, upon observing the experimental test data in Fig. 7 the total electrical impedance has a peak at approximately 9500 Hz, which indicates a capacitive effect on the electrical drive point impedance due to the drive coil. The coil in the Terfenol-D transducer is tightly wound insulated copper wire. The insulation is acting as a dielectric between windings which gives capacitive behavior to the coil. This capacitance is in parallel with the series combination of the coil resistance and inductance. The modified blocked electrical impedance is formed by this parallel combination and behaves as a bandpass filter

$$Z_e = \frac{R + j\omega L_{block}}{L_{block}C(j\omega)^2 + (RC + \alpha_{KV})j\omega + 1} \tag{27}$$

where the term $\alpha_{KV}j\omega$ is a Kelvin-Voigt correction factor that accounts for internal damping. Electrical resistance determines the amount of damping in the blocked electrical impedance. The drive coil has a DC resistance of 2 Ω and introduces very little electrical damping in the model.

The blocked mechanical expression found through derivation of the constitutive relations contains only a stiffness component and does not account for any inertia and damping effects of the Terfenol-D rod. The mechanical impedance of the transducer derived in Eqn. (3) is a more complete expression for the blocked mechanical impedance as it describes a second order system that considers the inertia, damping and stiffness effects of the effective Terfenol-D mass and is now used to describe the blocked mechanical impedance.

Load Impedance. In determining the electrical drive-point impedance Z_{ee} of the Terfenol-D transducer under loaded conditions, a load impedance Z_L due to the fluid loading is added to (17). The definition of the load impedance, Eqn. (15), provides a method for developing an expression for Z_L by relating it to the resultant force F on the transducer. Force F is defined in Eqn. (14) as the superposition of a term proportional to the applied current I and the product of the blocked mechanical impedance, defined by Eqn. (3), and the velocity v_t of the Terfenol-D transducer. Equations of motion (1)–(2) for the vibratory model of the Terfenol-D transducer are rewritten by noting that $\alpha = -T_{me}$ to obtain an equivalent expression for the resultant force F. This expression for F is used with the definition of the load impedance to yield an expression for Z_L in the frequency domain,

$$\begin{aligned} F &= T_{me}I + Z_mv_t = -Z_Lv_t \\ &= \frac{1}{2}\left[-(b_fj\omega + k_f)X_t + (b_fj\omega + k_f)X_f\right] \end{aligned} \tag{28}$$

$$Z_L = \frac{(b_fj\omega + k_f) - (b_fj\omega + k_f)\dfrac{X_f}{X_t}}{2j\omega}. \tag{29}$$

The load impedance is dependent on the ratio of fluid displacement to effective mass displacement. Equations (1)–(2) are represented in the frequency domain as a matrix equation and the variables X_t and X_f are solved by using Cramer's rule. The overall expression for the ratio of these two displacements is coupled to the system level matrix as the displacement variables are functions of the input current I and chamber pressure P_1. The inclusion of the load impedance concludes the required derivations of all aspects of the dynamic system model.

Full System Model and Simulations

Combining the modified expressions for blocked electrical and mechanical impedances, the transduction coefficients and the load impedance into Eqn. (17), the electrical drive point impedance is developed for the Terfenol-D transducer,

$$Z_{ee} = \frac{R + j\omega L_{block}}{L_{block}C(j\omega)^2 + (RC + \alpha_{KV})\, j\omega + 1} \qquad (30)$$
$$+ \frac{(Nqk_t)^2\, j\omega}{m_{eff}(j\omega)^2 + \left(b_i + \frac{1}{2}b_f\right) j\omega + k_i + \frac{1}{2}k_f - \frac{1}{2}\left(b_f j\omega + k_f\right)\frac{X_f}{X_t}}$$

where X_f/X_t couples the total electrical impedance frequency response function with the mechanical and fluid state space model through the chamber pressure P_1 and input current I. Since the state space portion of the model is solved in the time domain, a stepped sine simulation is written in which the state space system is solved for each frequency and concurrently inputs the corresponding chamber pressure and input current into the total electrical impedance. Simulations of the linear dynamic system model are presented in the results and discussion section.

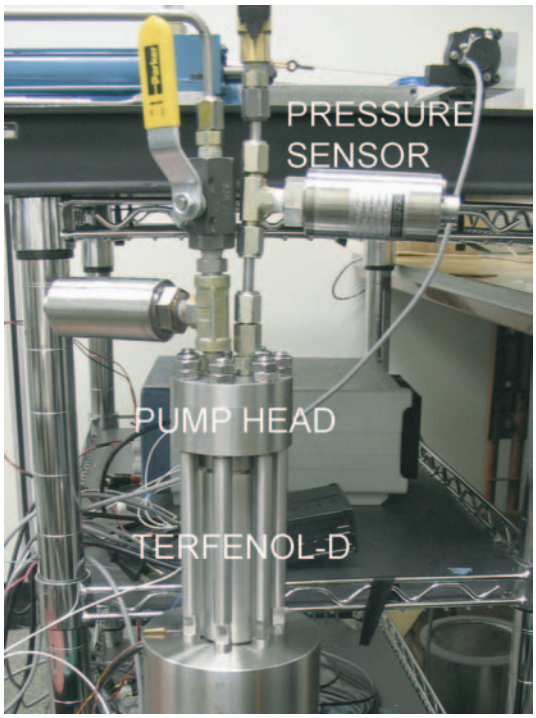

Figure 6. TERFENOL-D PUMP AND PRESSURE SENSORS.

EXPERIMENTAL SETUP AND TESTING

The harmonic and broadband testing performed on the transducer requires the same operating conditions in order to obtain meaningful data. Any air trapped inside the transducer will greatly reduce the efficiency of the pump, thus degassing of the hydraulic oil was employed for all tests. A vacuum pump degasses the hydraulic oil in the fluid network. The Terfenol-D pump is isolated from the vacuum because the seals in the pump are designed for external pressure. If exposed to a vacuum air will leak through the seals and continue to introduce air to the fluid. The pumping chamber is flushed with degassed hydraulic oil before testing which finishes the fluid preparation before testing. A prestress of 1 ksi and bias pressure of 250 psi are applied to the Terfenol-D rod and hydraulic circuit (Fig. 6). Operation under compression for the Terfenol-D rod protects the integrity of the rod and aligns the magnetic moments in a more energetically favorable orientation. The acceleration of the effective mass of the Terfenol-D rod, piston and diaphragm that will start to cause damage to the Terfenol-D is determined by $a_{max} = \sigma_{pre}A_t/m_i = 750$g's. Here, σ_{pre} is the prestress on the rod (1 ksi). The bias pressure of 250 psi is the pressure that produces optimal performance for the existing experimental setup.

Testing on the Terfenol-D pump characterizes the electrical drive-point impedance and determines the maximum attainable pressure and maximum no-load actuator velocity. Broadband testing of the Terfenol-D transducer is performed in order to quantify the electromechanical coupling of the transducer by obtaining the electrical impedance frequency response function. Swept sine tests are run from 10Hz-20kHz with a constant input voltage. The theoretical maximum attainable pressure of the Terfenol-D transducer occurs under blocked output conditions [1]. Tests are run under blocked output operating conditions for both with and without the output reed installed. Tests with the output reed removed allow for quantification of the pressure response of the pump by allowing the pressure to return to the bias pressure after each oscillation. Testing with the output reed valve installed quantifies the electromechanical coupling for the designed operation of the pump.

Harmonic pressure testing is performed under blocked output conditions. Two separate tests are performed. First, in order to quantify the frequency limitation of the reed valves, harmonic testing with 4 A peak to peak input is performed at various frequencies in an effort to trace the dynamic response of the pressure found through broadband testing. Secondly, to quantify the maximum pressure at a larger drive current, a 20 A peak to peak input waveform is held constant for each test.

Harmonic actuation testing of the EHA is performed for no applied load on the actuator. The displacement of the hydraulic cylinder is measured and the no-load velocity is determined by analyzing data after each test. The input current is a of 10 A peak to peak waveform. The no-load condition of the actuator permits larger amplitudes of the magnetostrictive vibrations which results in much larger accelerations. In order to assure that the acceleration does not unload the Terfenol-D rod, the input current is decreased which lowers the magnitude of the Terfenol-D vibrations and thus the acceleration.

RESULTS AND DISCUSSION

Broadband Testing and Model Simulation

Figures 7–8 show the electrical impedance frequency response function and model simulation for both tests. The broadband data without the output reed valve installed illustrates resonant activity at approximately 1600 Hz and 5060 Hz in the magnitude and phase of the electrical impedance illustrated by the 'Z' shape in the plots. The broadband pressure response, Fig. 9, shows a peak at 10 Hz followed by a decay in the pressure response and a larger peak at 1600 Hz. The tests with the output reed valve installed show only resonant motion at 5140 Hz; the peak at 1600 Hz is removed. This loss of transduction illustrates the change in loading between tests and indicates an increase in the loading on the Terfenol-D rod when the output reed valve is installed. When the reed is removed, the fluid dynamics of the pump head change and create an unobstructed output cavity that allows pressure waves to reflect off of each other and amplify the pressure response at 1600 Hz. When the output reed is installed, it prevents the fluid from acting in this manner. In both cases, the resonant motion near 5100 Hz is due to the mechanical resonance of the Terfenol-D pump.

A modification is made to the dynamic system model to simulate the blocked output conditions of these tests. The hydraulic cylinder in Fig. 1 is assumed to be attached to an infinite mass which would result in no actuator motion. A stepped sine simulation is performed on the dynamic system model using this modification. Frequencies from 10 Hz to 20 kHz are investigated with a frequency step of 50 Hz. The step is refined to 10 Hz near the location of the transducer resonance. The location of the resonance in the model is dependent on the values of two transducer properties, the Young's modulus $E_y^H = 1/s^H$ of Terfenol-D and the bulk modulus β of the hydraulic fluid, which are respectively proportional to the Terfenol-D stiffness k_t and fluid stiffness k_f. The Terfenol-D and fluid stiffness coefficients control the location of the motional component of the model. In order to obtain resonance near 5100 Hz, the values of the material properties E_y^H and β are determined in order to match the resonance of the experimental data. Lowering the bulk modulus, from the maximum value of 1.64 GPa provided by the manufacturer, becomes a measure of the effective bulk modulus β_{eff} of the chamber which accounts for any compliance that the model overlooks, such as any air remaining in the chamber or structural compliances. It is noted that the repeatability of the dynamic measurements is very high suggesting that the method of air removal is quite effective or that the slightest bit of air might be getting stuck somewhere inside the chamber every time. Changing the bulk modulus has a greater affect on the location of the transducer resonance and is lowered as needed while the Young's modulus of Terfenol-D typically is in the range of 25–35 GPa. The resulting combination of $E_y^H = 30$ GPa and $\beta = 0.93$ GPa produces the model frequency response function illustrated in Figs. 7–8 which are plotted against experimental data for comparison. The magnitude of the motional component is determined by the measure of the damping in the two degree of freedom model of the pump

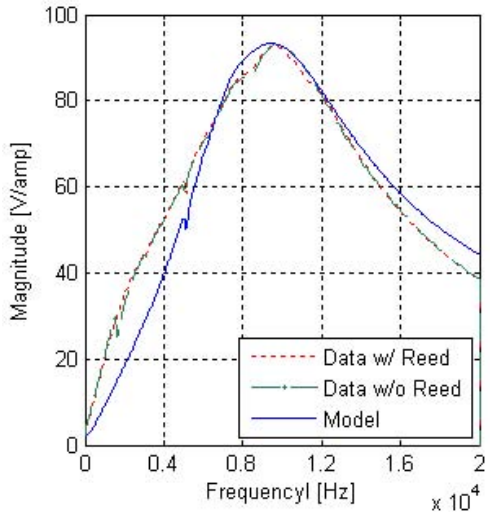

Figure 7. COMPARISON OF MODEL SIMULATION AND BROADBAND TESTING OF THE TERFENOL-D TRANSDUCER: (a) MAGNITUDE AND (b) PHASE RESPONSE OF THE ELECTRICAL IMPEDANCE Z_{ee}.

mechanical subsystem. The mechanical damping b_i of the pump has a more critical effect on the magnitude in that it must be held at a low value. For larger values of b_i, the 'Z' shape due to the motional component in the model is completely flattened out. The fluid damping b_f has an inverse effect on the motional component as compared to b_i. Increasing b_f increases the magnitude of the motional component. The corresponding mechanical and fluid damping ratios ζ_i and ζ_f that determine b_i and b_f and give the results in Figs. 7–8 are 0.09 and 0.55.

The large peak at 9500 Hz is the location of the electrical resonance of the coil due to the capacitive nature of the drive coil. The model calculates the inductance L_{block} through the mechanical and physical parameters of the Terfenol-D rod and the capacitance is calculated by the definition of electrical resonance,

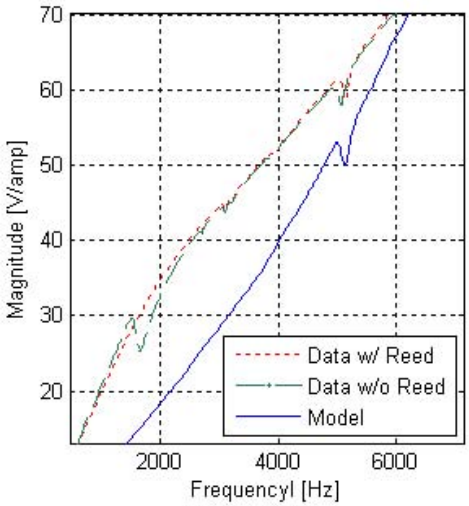

Figure 8. COMPARISON OF MODEL SIMULATION AND DYNAMIC TESTING OF THE TERFENOL-D TRANSDUCER: ZOOMED MAGNITUDE RESPONSE OF TOTAL ELECTRICAL IMPEDANCE.

$\omega_{coil} = 1/\sqrt{L_{block}C}$. The corresponding inductance L_{block} and capacitance C that give the location of this peak are 1.30 mH and 209 nF. The experimental data deviates from the model between 10 Hz to approximately 7000 Hz. The deviation is expected due to the numerous assumptions made during derivation of the linear model. Terfenol-D is a nonlinear material and is being modeled under the assumption that it operates over its pseudo-linear operating range. The model does not account for any turbulent or recirculation of the flow dynamics through the pump head and also ignores the inductance and capacitance of the fluid lines.

Harmonic Pressure Testing

Harmonic time domain testing is performed on the Terfenol-D pump under blocked output conditions. Fig. 9 shows the results from this harmonic testing alongside the stepped-sine pressure response. The blocked harmonic tests follow the trend of the dynamic pressure trace up until 1000 Hz where a drop in frequency occurs. The reed valves were designed in air to have a natural frequency of approximately 3000 Hz. The drop in the range of usable frequencies for the reed valves is due to the shear loading effects of the hydraulic fluid.

The second set of blocked harmonic tests is to quantify the maximum blocked output pressure for a drive current of 10 A amplitude. Frequencies between 1 Hz and 100 Hz are tested for the Terfenol-D pump. The maximum pressure of 1100 psi above the bias pressure occurs at 10 Hz with a power consumption of 83.8 W. The pressure differential peaks at 10 Hz then decays as the frequency is increased, consistent with previous data. The input power is calculated by $P_{in} = V_{RMS} I_{RMS} \cos\theta$, where the phase θ between the RMS voltage and current is obtained for each frequency by the phase response of Z_{ee} provided in Figure 7(b).

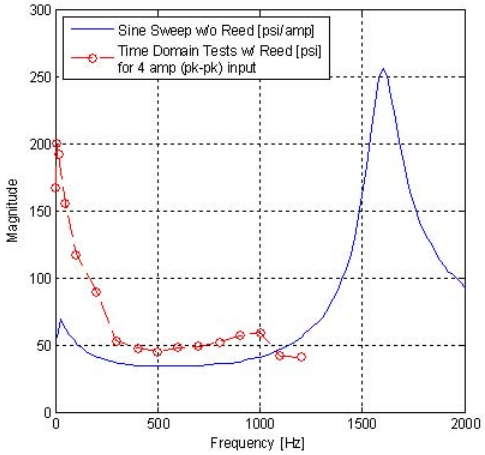

Figure 9. HARMONIC BLOCKED PRESSURE TESTING ALONGSIDE DYNAMIC PRESSURE DATA. HARMONIC TESTING LOCATES THE FREQUENCY LIMITATION OF THE REED VALVES AT 1000 HZ.

A time trace at 10 Hz for the dynamic system model is performed using the system variables identified during the broadband testing of the transducer and model. Figure 10 illustrates the time traces of the output pressure P_3 of the model and the blocked pressure of the Terfenol-D transducer for a 10 Hz/10 A sinusoidal input. The experimental data shows small spikes in the pressure trace, which occur at 10 Hz. These spikes in the data are due to pressure leaking back into the chamber before the reed valve is fully closed. The magnitude of the leakage in the steady state region of the pressure trace is 40 psi. The model captures the trend of the harmonic data but lacks the pressure 'recoil' that is present in experimental data. The algorithm describing the fluid diode behavior in the model does not account for the pressure leaking beneath the reed as it is closing.

Harmonic No-Load Testing

The main focus of the harmonic no-load actuation tests is to locate the frequency limitation of the EHA and also quantify the maximum no-load velocity. An input current of 5 A amplitude is held constant for each test. Frequencies were tested up to 200 Hz. There is a steep drop off in actuator velocity after 165 Hz with a peak at 160 Hz of 0.365 in/s. It is noted that the tests at or below 165 Hz have repeatable results but the same cannot be said for frequencies above 165 Hz where the discrepancy between tests is quite significant. The hydraulic cylinder used in these tests has a maximum operating pressure of 2320 psi with a 25 mm bore and 18 mm rod. The high pressure sealing of the piston contributes a large amount of friction to the actuator and increased difficulty in manually moving the piston is experienced when a bias pressure is applied to the hydraulic fluid. As illustrated in Fig. 9 in the harmonic pressure response, a peak in the pressure response occurs at 10 Hz and the pressure produced between 165–200 Hz is not enough to overcome the force of friction in the hydraulic

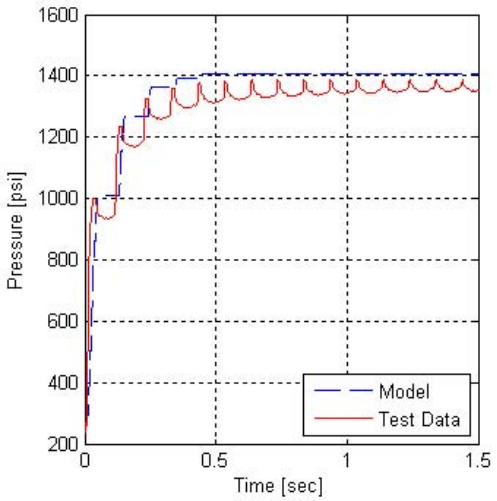

Figure 10. PRESSURE TRACE IN THE TIME DOMAIN FOR MODEL SIMULATION AND HARMONIC TEST FOR A 10 HZ / 10 A SINUSOIDAL INPUT.

cylinder. The nonuniform force of friction accounts for the erratic behavior above 165 Hz. 165 Hz is the frequency limitation of the EHA but is not the limitation of the Terfenol-D pump.

CONCLUDING REMARKS

A linear dynamic system model of the Terfenol-D pump is developed which couples the electrical, mechanical and fluid regimes of the pump; it predicts the maximum pressure of the Terfenol-D pump and predicts the location of the transducer resonance along with the broadband characteristics up to 20 kHz. The model identifies important system parameters of the pump that could not be known otherwise, such as the effective bulk modulus, Young's modulus, damping ratios and drive coil capacitance. The model does not account for any turbulent effects or recirculation of the flow dynamics through the pump head and also ignores the inertia and capacitance of the hydraulic fluid in the fluid lines. Although the deviations from the linear dynamic system model and experimental data seem significant, the model accurately describes the locations and magnitudes of the motional component of the Terfenol-D pump. The Terfenol-D pump produces a maximum steady-state pressure differential of 1100 psi at 10 Hz and 83.8 W. The shear loading effects of the hydraulic oil slow the response of the reed valve creating a leakage in the pressure trace due to fluid escaping beneath the reed as it closes. A lighter hydraulic fluid will decrease the effects of the shear loading due to the fluid, increase the reed valve response and at the same time reduce the amount of pressure leakage as the reed valve is closing. The reed valves have a maximum operational frequency of 1000 Hz. The EHA provides a maximum no-load velocity of 0.365 in/s at 160 Hz and has a frequency limitation at 165 Hz. The hydraulic cylinder used in the EHA introduces a large amount of nonuniform friction to the EHA, which severely limits its performance.

ACKNOWLEDGMENT

The authors wish to acknowledge Gerry McCann of DANA Corp., Commercial Vehicle Systems, and Dr. Julie Slaughter of Etrema Products, Inc.

REFERENCES

[1] Bridger, K., Sewell, J.M., Cooke, A.V., Lutian, J.L., Kohlhafer, D., Small, G.E., and Kuhn, P. M., 2004. "High-pressure magnetostrictive pump development: a comparison of prototype and modeled performance". In Smart Structures and Materials 2004: Industrial and Commercial Applications of Smart Structures Technologies, E. H. Anderson, ed., Vol. 5388 of *Proc. SPIE*, pp. 246–257.

[2] Sirohi, J., and Chopra, I., 2003. "Design and development of a high pumping frequency piezoelectric-hydraulic hybrid actuator". *Journal of Intelligent Material Systems and Structures*, **14**, pp. 135–147.

[3] E.G. Chapman, S.L. Herdic, C.A. Keller, and Lynch, C.S., 2005. "Development of miniaturized piezo-hydraulic pumps". In Smart Structures and Materials 2005: Industrial and Commercial Applications of Smart Structures Technologies, E. V. White, ed., Vol. 5762 of *Proceedings of SPIE*, pp. 299–310.

[4] Oates, W.S., and Lynch, C.S., 2001. "Piezoelectric hydraulic pump system dynamic model". *Journal of Intelligent Material Systems and Structures*, **12**, pp. 737–744.

[5] Sirohi, J., C. Cadou, and Chopra, I., 2005. "Investigation of the dynamic characteristics of a piezohydraulic actuator". *Journal of Intelligent Material Systems and Structures*, **16**, pp. 481–492.

[6] Downey, P.R., and Dapino, M.J., 2005. "Extended frequency bandwidth and elictrical resonance tuning in hybrid terfenol-d/pmn-pt transducers in mechanical series configuration". *Journal of Intelligent Material Systems and Structures*, **16**, pp. 757–772.

[7] Shearer, J.L., Kulakowski, B.T., and Gardner, J.F., 1997. *Dynamic modeling and control of engineering systems*, 2nd edition ed. Prentice Hall.

[8] Auslander, D.M., Takahashi, Y., and Rabins, M.J., 1974. *Introducing Systems and Control*. McGraw-Hill.

[9] Hunt, F.V., 1982. *The Analysis of Transduction, and Its Historical Background*. American Institute of Physics for the Acoustical Society of America.